minerals

Article

Carbon Dioxide Sorption Isotherm Study on Pristine and Acid-Treated Olivine and Its Application in the Vacuum Swing Adsorption Process

Jiajie Li and Michael Hitch *

Norman B. Keevil Institute of Mining Engineering, University of British Columbia, 517-6350 Stores Road, Vancouver, BC V6T 1Z4, Canada; E-Mail: jiajie.li@alumni.ubc.ca

* Author to whom correspondence should be addressed; E-Mail: mhitch@mining.ubc.ca; Tel.: +1-604-827-5089; Fax: +1-604-822-5599.

Academic Editor: Tuncel M. Yegulalp

Abstract: This paper investigates the potential of pristine and acid-treated olivine as a substrate for CO_2 capture using a vacuum swing adsorption (VSA) process from the gas-solid phase. The experiments tested the isotherm of pure CO_2 adsorption with partial pressure from 10^{-5} to 1 bar at ambient temperature. The CO_2 adsorption capacity and actual expected working capacity (EWC) curves of pristine and acid-treated olivine were determined. Isotherm studies predict that physisorption dominates chemisorptions at ambient temperatures. The adsorption capacity enhances with the increase of specific surface area, pore volume, and the appearance of Mg complexed on the mineral's surface. Actual EWC studies showed that acid-treated olivine is an adsorbent choice for the VSA process, due to enhanced CO_2 adsorption capacities compared to olivine and the potential for 100% recovery of CO_2 during the regeneration process. Pristine olivine is not suitable for the VSA process because of bad regenerability, but it can be used in capturing and sequestering dilute CO_2 in process streams. Our research reveals excellent viability for the application of VSA in the area of CO_2 capture using pristine olivine and acid-treated olivine.

Keywords: vacuum swing adsorption; isotherm; olivine; actual expected work capacity

1. Introduction

The rapid increase of carbon dioxide (CO_2) concentration in the atmosphere by human activities has led to serious environmental problems, such as global warming and ocean surface acidification [1]. Carbon dioxide capture and sequestration (CCS) is generally recognized as the quickest and the most environmentally benign way of reducing CO_2 concentration at present [2]. CCS generally involves CO_2 separation from the flue gas of power plants or natural gases, and then storage in geological reservoirs. In recent years, research interests have come to integrate CO_2 capture with CO_2 sequestration [3–7]. In all CO_2 sequestration methods, CO_2 mineral sequestration can guarantee the permanent and environmentally-friendly storage of CO_2 [8]. One possible way of combining CO_2 capture and sequestration is through the use of mineral-adsorbents for CO_2 separation [7,9].

CO_2 separation can be achieved by CO_2 adsorption in either dry or aqueous conditions [10]. In dry conditions, CO_2 molecules are chemically adsorbed onto a solid by strong chemical bonds or physically adsorbed by weaker inter-molecular bonds [10]. The CO_2 adsorption capacity of adsorbents relies on the temperature, the CO_2 partial pressure, and the interaction potential between the CO_2 and the adsorbent itself [11]. In aqueous conditions, CO_2 is dissolved into the solvent first, and then is reacted with adsorbent [12]. According to the options for CO_2 regeneration or desorption, there are 3 typical CO_2 separation methods, namely pressure swing adsorption (PSA), temperature swing adsorption (TSA) and electrical swing adsorption (ESA) [10]. PSA is favored in all the CO_2 separation methods, not only because of its process simplicity and cost efficiency, but also due to its rapid pressure changes, which meet the requirements for fast adsorption and effective regeneration. However, longer time adsorption steps under low gas concentration may favor other operations, such as TSA [10]. Vacuum swing adsorption (VSA) derivates from PSA. In VSA, one or more gases are favorably adsorbed at atmospheric pressure or slightly higher than atmospheric pressure (1–1.5 bar) and then desorbed or regenerated at a vacuum pressure (typically 0.01–0.1 bar) [13]. The VSA is much simpler and cheaper than PSA, due to the absence of a pressurization step. However, the challenge of CO_2 capture by VSA is the search for suitable adsorbents for CO_2 separation. Favorable adsorbents need to have a high CO_2 adsorption capacity, high CO_2 selectivity, fast adsorption kinetics, low-energy requirement for desorption, stable adsorption-desorption cycles, tolerance to moisture and impurities, and low energy requirements [14]. Micropore physisorbents (Zeolites, carbon molecular sieves, metal organic frameworks, microporous polymers), mesopore physisorbents (mesopore silica, activated carbon), and amine-modified chemisorbents have been studied in the VSA processes [15,16]. Sayari *et al*. [14] found that most physisorbents were suitable at low temperature and high pressure, but they are not tolerant to moisture. On the contrary, chemisorbents can adsorb large amounts of CO_2 at low pressure, adsorb/desorb rapidly, and have a high tolerance to moisture.

Magnesium/calcium-based minerals have been considered as sorbents for CO_2 separation [17]. Magnesium and calcium are naturally available as silicate or aluminosilicate. Magnesium silicates, such as olivine and serpentine, are the most abundant feedstock available globally [18] and the predominant tailings minerals for ultramafic-hosted nickel, PGE and diamond deposits [19]. Magnesium silicates are attractive for CO_2 separation in coal-fired power plants, due to their ability to adsorb CO_2 under relatively high temperatures (<200 °C), and to enhance CO_2 adsorption capacity in the presence of moisture [20]. Low CO_2 pressure and high temperature can help obtaining a high CO_2

adsorption capacity for magnesium silicate [5,6]. Various pretreatment methods, including mechanical, thermal, and chemical activation, could change the specific surface area and crystal structure of minerals, thus enhancing the CO_2 adsorption capacity under ambient operation conditions near room pressure and temperature [21]. Up to now, research has suggested that the optimum product in chemical activation on magnesium silicates is sulfuric acid-treated serpentine, which is a mesopore product with a specific surface area of 330 m^2/g [22]. A number of papers on the chemical and morphological changes as a result of CO_2 interactions with olivine have been published [23–27]. However, mineral-based sorbents are rarely tested in the VSA process [28]. To better understand what factors control the VSA process, it is important to develop a fundamental study on the mechanism of CO_2 adsorption on the surface of these minerals as well as their pretreated materials.

The present study involves an examination of pure CO_2 adsorption isotherm on pristine and acid-treated olivine and their expected working capacities (EWC). Pristine olivine and acid treated olivine are chosen, because they are cheap and readily available in the form of milled tailings offering a suitable and cost-effective substrate CO_2 mineral separation and sequestration in a modified mineral processing facility. The main objective of this research was to demonstrate the physical and chemical advantages of the typical mine waste materials as adsorbents for removing or storing CO_2 using a single VSA process under ambient temperature. The results of such a study will provide information for future process optimization and design.

2. Material and Experiments

2.1. Materials Preparation

The current study was carried out on olivine samples from the Twin Sisters Deposit in northwest Washington State, USA. Based on results obtained from the Rietveld analysis on X-ray powder diffraction patterns, the sample contained approximately 97.9 wt% forsterite olivine (Mg_2SiO_4), 0.2 wt% lizardite ($Mg_3Si_2O_5(OH)_4$), 1.5 wt% chromite ($FeCr_2O_4$), and 0.4 wt% quartz (SiO_2). The quantitative XRD analysis was done by the Department of Earth and Ocean Sciences, UBC (The University of British Columbia) [29]. The olivine samples were ground by hand in a set of laboratory agate (99.91%) mortar and pestle to prevent contamination. The ground product was screened in a 106 mesh sieve. The particles that passed the sieve had an 80% passing size of 91.1 ± 2.9 μm with a specific surface area of 0.61 ± 0.04 m^2/g, which was the pristine olivine sample for CO_2 sorption tests.

2.2. Experimental Procedure

Exactly 10 g pristine olivine (OL) was leached in 100 mL HCl acid solution at room temperature for 30 min. Acid concentrations of 0.25, 0.5, 1 and 5 M were applied. A magnetic stirrer operating at a speed of 400 rpm was used for mixing during leaching. The solutions in equilibrium with the acid-treated olivine (OL-A) were rinsed with de-ionized water until solutions reached a neutral pH. The pH was measured by a pH electrode and voltmeter. Solids were separated over millipore filters (0.45 μm Type HAMP, EMD Millipore Corporation, Merck KGaA, Darmstadt, Germany), dried in an oven at 100 °C for 12 h and sampled for CO_2 sorption testing. Since the melting temperature of

forsterite olivine is 1900 °C [30], being dried in 100 °C will not alter the olivine and its absorption properties. The acid treatment procedure followed that of Maroto-valer *et al.* [22]. The textural properties of pristine and acid-treated olivine were characterized by N_2 adsorption at 77 K on Autosorb-1MP (Quantachrome Instruments, Boynton Beach, FL, USA). The specific surface area was obtained using the Brunauer-Emmett-Teller (BET) method. The micropore volumes (<2 nm) were calculated using the Dubinin-Radushkevitch (D-R) equation to the N_2 adsorption isotherm at relative pressure (P/P_0) less than 0.1 and mesopore volumes (2–50 nm) were calculated from the application of the Barrett-Joyner-Halenda (BJH) equation to the N_2 adsorption isotherm at $0.1 < P/P_0 < 1$. Where, P is the pressure of N_2 and P_0 is the saturation pressure of N_2 at 77 K. The total pore volume was calculated by adding up the micropore volume and mesopore volume.

The grain morphologies of OL and OL-A were examined using a Zeiss Supra-55 scanning electron microscope (SEM) with a secondary electron detector at 15 kV (Zeiss, Oberkochen, Germany). The semiquantitative chemical analysis was done by the Zeiss Supra-55 SEM equipped with a light element energy-dispersive X-ray spectroscope (EDS). Samples were attached on carbon tabs prior to SEM analysis.

CO_2 sorption tests on materials by volumetric methods were also operated on the Autosorb-1 analyzer (Quantachrome Instruments) at 298 K. The samples were degassed at 298 K prior to CO_2 adsorption analysis, in order to obtain a clean surface. The overall isotherm contained 75 adsorption points and 39 desorption points at standard spacing for a relative pressure range of 10^{-5} to 1 bar. A minimum equilibrium interval of 3 min for pressure from 10^{-5} to 1 bar was used for each measurement point equilibrium determination. These high resolution measurements led to acceptable accuracy of CO_2 adsorption capacity measurements.

3. Results

3.1. Characteristics of Pristine and Acid-Treated Olivine

Acid treatment changes the physical property of olivine. Table 1 lists the textural characteristics of olivine treated by various acid concentrations (C_{HCl}). Initially, the specific surface areas (S_{BET}) of acid-treated olivine increase with C_{HCl} and then decrease. OL-A1 exhibited the largest S_{BET} at 2.79 m^2/g. The changes of micropores ($P_{V-micro}$) and mesopores (P_{V-meso}) are similar to the specific surface area.

Table 1. Specific surface area and porosity properties of pristine and acid-treated olivine.

Material	C_{HCl} (M)	S_{BET} (m^2/g)	$P_{V-micro}$ ($\times 10^{-3}$ cm^3/g)	($\times 10^{-3}$ cm^3/m^2)	P_{V-meso} ($\times 10^{-3}$ cm^3/g)	($\times 10^{-3}$ cm^3/m^2)	$P_{V-total}$ ($\times 10^{-3}$ cm^3/g)	($\times 10^{-3}$ cm^3/m^2)	A_{CO_2}[a] (mg/g)	(mg/m²)
OL	0	0.55	0.18	0.33	1.55	2.8	1.73	2.73	0.15	0.27
OL-A0.25	0.25	1.29	0.44	0.34	2.36	1.83	2.80	2.02	0.10	0.08
OL-A0.5	0.5	2.2	0.79	0.36	2.14	0.97	2.93	1.14	0.25	0.11
OL-A1	1	2.79	1.10	0.39	2.23	0.8	3.33	1.08	0.26	0.09
OL-A5	5	1.16	0. 38	0.33	1.76	1.52	2.14	1.72	0.16	0.14

a, A_{CO_2} is the adsorption capacity at 1 bar, (mg CO_2/g material) or (mg CO_2/m² material).

Figure 1 shows the micropore volume and mesopore volume per unit surface area as a function of acid concentration. The micropore volumes range from 0.00033 to 0.00039 cc/m^2, and remains nearly constant after acid leaching. In other words, the micropore volumes per unit surface area remain independent of the acid concentration. The mesopore volume decreased linearly at acid concentrations lower than 1 M HCl, and slightly increased at higher acid concentrations (*i.e.*, 5 M HCl). The changing trends of total pore volumes ($P_{V\text{-total}}$) were determined by the resulting mesopore volumes (see Table 1). Hence, 1 M seems the optimum HCl concentration for increasing the specific surface area and total pore volume, but results in a product with the lowest pore volume per unit surface area.
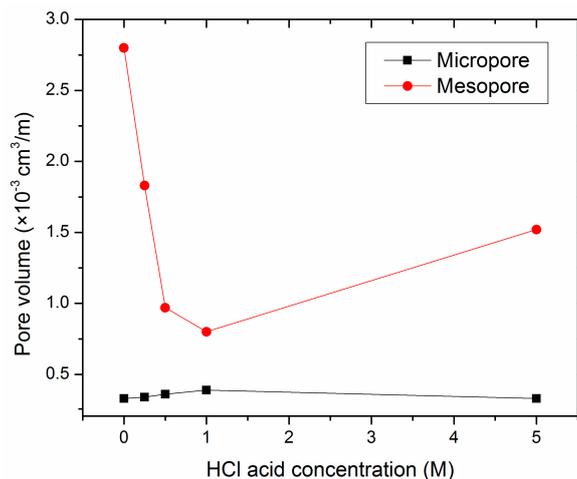

Figure 1. Micropore (■) and mesopore (●) volume as a function of specific surface area.

Table 1 shows that the CO_2 adsorption capacity (A_{CO2}) at 1 bar of acid-treated olivine varies with the change in specific surface area and pore volume. However, although the specific surface area of OL-A0.25 is larger than OL, A_{CO2} is decreased slightly. The analysis adopts A_{CO2} per unit surface area to estimate the CO_2 adsorption affinity on the solid surface. Figure 2 shows that CO_2 adsorption capacity per unit surface area of OL is about three times that of OL-A. A_{CO2} on OL-A increases slightly with a slope of 0.011 as the acid concentration increases. Specific surface area is not the only factor that determines A_{CO2}.
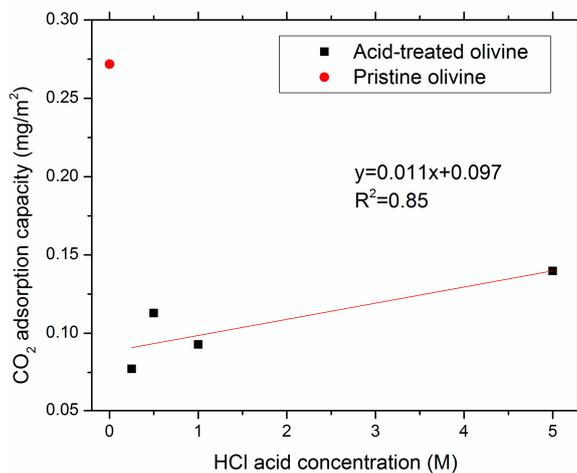

Figure 2. Correlations between acid concentration and CO_2 adsorption capacities per unit surface area.

Figure 3a,c are the SEM micrographs of olivine (OL) and 0.25 M HCl leached olivine (OL-A0.25). The shape of the particles have no significant difference between both micrographs, through Figure 3a is more fractured than Figure 3c. Figure 3c appears to have some charging and the bright areas represent areas of heavy elements. Figure 3b,d are representative EDS spectra of olivine (OL) and 0.25 M HCl leached olivine (OL-A0.25), respectively. The average EDS results from ten points on each sample indicate that the ratio of Mg:Si decreased from 1.78 to 1.27 after 0.25 M HCl acid treatment. The ratios of Mg:Si are 1.20, 1.23 and 1.19 on the olivine after being leached in 0.5, 1 and 5 M HCl acid, respectively. The constant Mg:Si ratios demonstrate that the surface chemistry of acid-treated olivine is independent of the acid concentration from 0.5–5 M. The loss of Mg complexed on the mineral's surface may be the reason for reduction in A_{CO_2} per unit surface area on olivine after acid leaching [31].
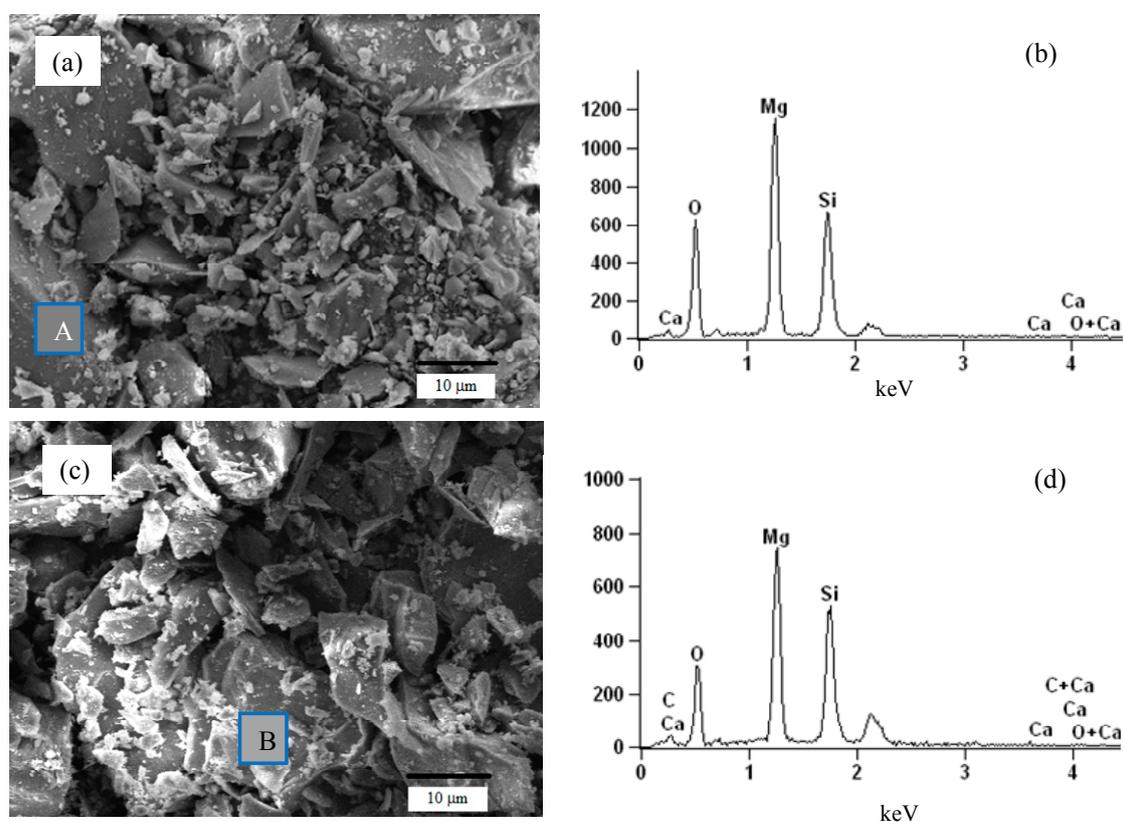

Figure 3. (**a**) SEM micrograph of olivine (OL); (**b**) Energy-dispersive X-ray spectroscope (EDS) spectra of region A; (**c**) SEM micrograph of 0.25 M HCl acid-treated olivine (OL-A0.25); (**d**) EDS spectra of region B. Region A and B are marked on (a) and (c) respectively.

3.2. CO2 Sorption Isotherm Profiles

An adsorption study on pristine and acid-treated olivine was performed based on CO_2 adsorption capacity. Figure 4 shows the CO_2 sorption isotherms obtained at 25 °C. The points stand for the experimental data, and the curves correspond to the regressed form of the Freundlich isotherm. Except for the CO_2 desorption isotherm on OL, all the other isotherms visually fit the Freundlich isotherm quite well.
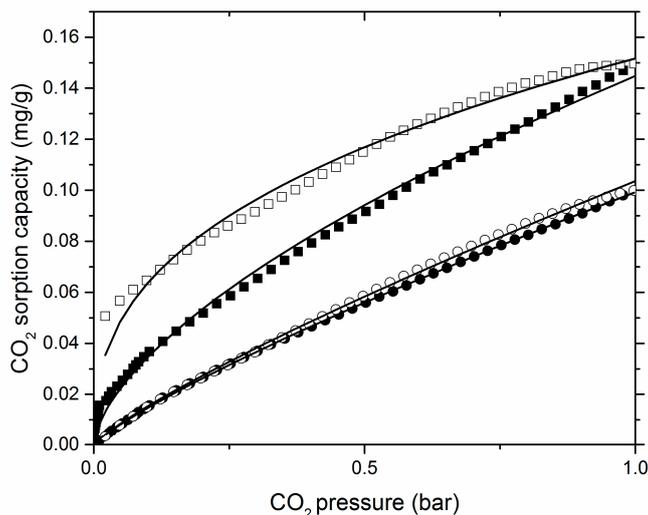
Figure 4. CO_2 adsorption isotherms on OL (■) and OL-A0.25 (●), desorption isotherm on OL (□) and OL-A0.25 (○) at 25 °C.

The shape of the CO_2 adsorption isotherm curve on OL is an IUPAC (International Union of Pure and Applied Chemistry) type II isotherm [11], which commonly accounts for multilayer adsorption on materials having a comparatively low porosity. An inflection point occurs at around a CO_2 partial pressure (P_{CO2}) of 0.01 bars under our experimental conditions, presenting the end of the first layer coverage and the start of multilayer adsorption. However, the CO_2 adsorption isotherm on OL-A0.25 demonstrates a nearly linear relationship between P_{CO2} and A_{CO2}.

Figure 4 also reveals that the CO_2 desorption isotherm does not coincide with its adsorption isotherm on pristine olivine, indicating the irreversible nature of CO_2 with the VSA process at ambient temperatures. The desorption gap at P_{CO2} of 0.02 bar was about 20% of A_{CO2} at 1 bar. Alternately, a reversible sorption of CO_2 on acid-treated olivine was observed.

3.3. Mathematical Analysis of the CO_2 Sorption Isotherms

3.3.1. CO_2 Sorption Isotherm Models

Many isotherm models have been developed for gas adsorption on solids surface [11]. For convenience, explicit and simple models are generally preferred and commonly used [32]. Table 2 lists four popular isotherm models for gas adsorption and microporous adsorbents that have been adopted in this research. The aim was to find a suitable model to fit the experimental data for the calculation of expected working capacity. The Langmuir model describes the formation of monolayer adsorbate on a completely homogeneous surface. On the other hand, the Freundlich isotherm is purely empirical and commonly used for highly heterogeneous surfaces. The Dubinin-Radushkevich isotherm also focuses on the non-uniform surfaces, though it specifically considers the Gaussian energy distribution on the surface of adsorbents. The Temkin isotherm explicitly addresses the adsorbent-adsorbate interaction, with a uniform distribution of binding energy and assumes that adsorption heat is simply a linear function of surface coverage [11].

Table 2. Four isotherm models adopted in this work and their parameters.

Isotherms	Models	Energy Parameters	Parameters in Equation
Langmiur	$a = \dfrac{a_m k_l P}{1 + k_l P}$	-	k_l is the Langmuir adsorption constant; a_m is the monolayer capacity (cc/g)
Freundlich	$a = k_f P^{1/n}$	-	k_f is the parameters of Freundlich model; n is adsorption intensity
Dubinin-Radushkevich	$a = a_0 e^{-b(RT\ln(1+1/p))^2}$	$E = \dfrac{1}{\sqrt{2b}}$	a_0 is the number of moles of adsorbate required to fill the micropores (mg/g); b is the D-R isotherm constant (mol^2/kJ^2)
Temkin	$a = \dfrac{RT}{b_T}\ln(a_T + P)$	$B = \dfrac{RT}{b_T}$	a_T is the Temkin isotherm equilibrium binding constant (cc/g); b_T is the Temkin isotherm constant

a is the adsorption capacity (cc/g); P is the CO_2 pressure (bar); R is the gas constant (8.314 J/(mol·K)), T is the absolute temperature (K); E is the mean free energy (kJ/mol), B is the constant related to the heat of sorption (J/mol).

3.3.2. Model Fitting of the CO_2 Sorption Isotherm

Table 3 lists the fitted parameter values of four models on CO_2 adsorption and desorption isotherms of pristine and acid-treated olivine. The correlation coefficient R^2 indicates all four isotherm models' fit remains acceptable in Table 3.

Table 3. The fitted parameter values using different adsorption isotherm models.

Isotherm Model	Parameter	OL		OL-A0.25	
		CO$_2$ Adsorption	CO$_2$ Desorption	CO$_2$ Adsorption	CO$_2$ Desorption
Langmiur	a_m	0.145	0.099	0.194	0.203
	k_l	1.182	4.296	0.388	0.386
	R^2	0.995	0.962	1.000	1.000
Freundlich	k_f	0.080	0.084	0.055	0.058
	n	1.610	2.655	1.209	1.206
	R^2	0.999	0.992	1.000	0.999
Dubinin-Radushkevich	a_0	0.085	0.084	0.064	0.069
	b	0.328	0.169	0.519	0.554
	E	1.235	1.720	0.981	0.950
	R^2	0.984	0.933	0.992	0.990
Temkin	a_T	1.039	1.333	1.002	0.999
	b_T	21,079.803	23,903.631	31,779.675	30,402.608
	B	0.118	0.104	0.078	0.081
	R^2	0.995	0.996	1.000	1.000

Although all equilibrium models display a good fit with the experimental data, the Freundlich isotherm presents the best description of CO_2 adsorption on pristine olivine and gives the maximum R^2 value among all the models used. The Dubinin-Radushkevich isotherms conversely have poor fits for both CO_2 isotherms on pristine and acid-treated olivine. With the exception of the

Dubinin-Radushkevich, all other models have an R^2 of 100% for the CO_2 adsorption isotherm on acid-treated olivine. Based on the results of this study, the best isotherm models fit for CO_2 adsorption on pristine olivine follow the order, from best to worst, of Freundlich, Temkin, Langmiur, and the Dubinin-Radushkevich isotherm.

The isotherm models provide some information about adsorption mechanisms. The Dubinin-Radushkevich and Temkin isotherms contain energy parameters: present mean free energy (*E*) and heat of sorption (*B*). The two energy values were estimated as 1.24 kJ/mol and 0.12 J/mol for pristine olivine, and 0.981 kJ/mol and 0.08 J/mol for 0.25 M HCl treated olivine respectively. These two energy values can predict the types of adsorption. An *E* value of less than 8 kJ/mol and a *B* value of less than 20 J/mol is an indication of physisorption dominating chemisorptions and ion exchange [33]. The CO_2 adsorption mechanisms on pristine and acid-treated olivine are physisortion mechanisms.

The Temkin model describes CO_2 desorption on pristine olivine most closely, followed by the Freundlich, Langmiur, and Dubinin-Radushkevich models. Homogeneous adsorbent-adsorbate interactions appears to be important during the vacuum desorption process. The *B* value (*i.e.*, heat of sorption) in the Temkin model for the CO_2 desorption isotherm is 0.104 J/mol, which is 0.014 J/mol lower than that for the CO_2 adsorption isotherm. The decrease in *B* value correlates to a reduction in CO_2 desorption and indicates a delay in CO_2 desorption on the surface of pristine olivine. Similarly, the *B* value for CO_2 adsorption remains the same as or 0.003 J/mol higher than CO_2 desorption on the acid-treated olivine, confirming a reversible process of CO_2 sorption. A reversible adsorption is often preferred in the VSA process.

3.4. CO₂ Expected Working Capacity

High CO_2 adsorption capacity is a requirement for adsorbents selected for CO_2 separation, and simple regeneration under depressurization is a critical criterion. Expected working capacity (EWC) is usually used to effectively estimate the performance of adsorbents in a separation process considering both CO_2 adsorption capacity and regeneration [34].

EWC has been used as a simple and sufficient indicator of performance in swing adsorption cycles [16]. The EWC describes the differences in CO_2 adsorption capacities between feed and regeneration condition. EWC can only be calculated through the adsorption isotherm, when the adsorption and desorption isotherms coincide. In the case of irreversible adsorption, such as CO_2 adsorption on pristine olivine, EWC should consider both the adsorption and desorption isotherms. Figure 5 explains the volumetric sorption isotherm and EWC for a VSA on OL, when CO_2 feed is at a partial pressure of 1 bar and regenerating at 0.1 bar. The actual working capacity is lower than the working capacity calculated by the adsorption isotherm alone. In this study, the EWC calculation is based on the Freundlich isotherm.

OL and OL-A5 were chosen for their EWC comparison, because they have similar amounts of CO_2 adsorption capacity per gram. Figure 6 shows the comparison of EWC on OL and OL-A5, when considering the CO_2 adsorption isotherm only. The EWC of OL and OL-A5 intersect with each other under certain feed and regeneration pressures. The intersections follow a linear relationship, which is expressed by a solid line in Figure 6. To obtain a high EWC, OL is suitable for low pressure and

OL-A5 for high pressure. OL may be an ideal candidate for diluted CO_2 removal in mining industry practice.
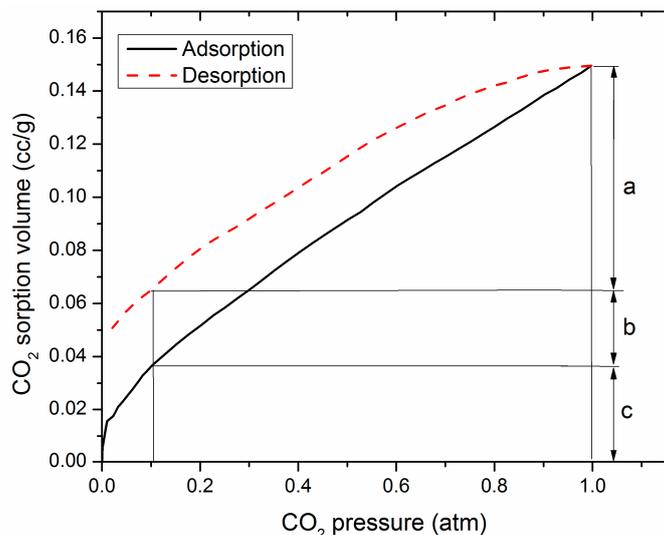

Figure 5. Demonstration of capacity and working capacity for vacuum swing adsorption (VSA) on OL (a): actual working capacity; (a + b): adsorption isothermal working capacity; (a + b + c): absolute capacity.
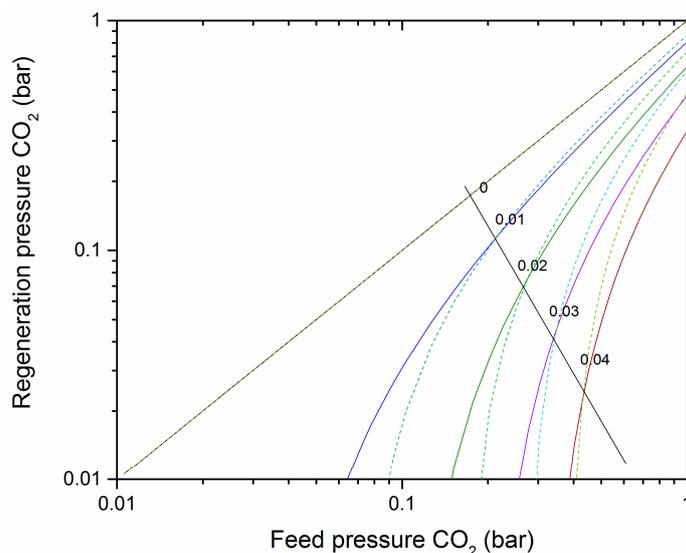

Figure 6. Adsorption isotherm expected working capacity (EWC) contours (mg/g) for CO_2 with OL (solid line) and OL-A5 (dash line) CO_2 under equilibrium condition at 25 °C.

A comparison of the actual EWC on OL and OL-A5 displays no intersections as shown in Figure 7. OL-A5 maintained a high EWC under relatively low adsorption pressure and high regeneration pressure. This means that OL-A5 may be an adsorbent choice for CO_2 separation in mining industry practice.
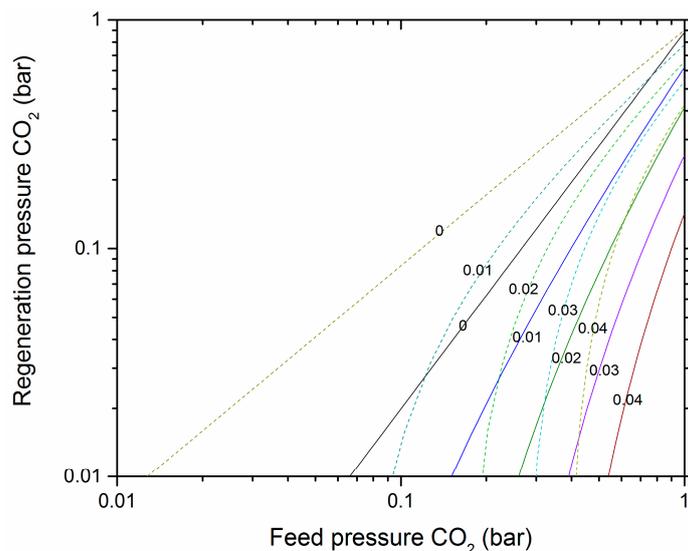
Figure 7. Actual EWC contours (mg/g) for CO_2 with OL (solid line) and OL-A5 (dash line) under equilibrium condition at 25 °C.

4. Discussion

4.1. The Effect of Leaching on Olivine Surface

As previously indicated, the initial olivine is more fractured than acid-treated olivine in SEM micrographs (Figure 3). The loss of small particles may be due to the fine particles that can be dissolved in acid quickly. This is in agreement with the pretreatment of olivine by mechanical activation, which generates a greater amount of fines in order to accelerate the downstream leaching and carbonation process [35]. However, the specific surface area and total pore volume increases after acid treatment. This is because the process of acid treatment creates micropores, collapses the adjacent walls of the micropores, and then forms wider pores, *i.e.*, mesopores. Figure 2 shows that the CO_2 adsorption capacity per surface area on acid-treated olivine is nearly unchanged. It means that the interaction potential between CO_2 and the surface of a material is constant. In this case, the CO_2 adsorption capacity has a linear relation with the specific surface area of the material. Olivine leached in 1 M HCl acid shows that the largest specific surface area in all the other acid concentrations is also the optimum sample preperation condition for CO_2 adsorption.

The CO_2 adsorption capacity per surface area on pristine olivine is three times greater than that of acid-treated olivine. The surface chemistry may be the main reason for the differences. EDS spectra show that the magnesium on olivine surfaces is lost after acid treatment. This is in line with previous results in which Mg was washed out, and a porous silica passive layer was left on the surface of the olivine during acid leaching [36]. The Mg:Si ratios on the surface of acid-treated olivine are independent of the acid concentration. This finding is counter to various studies on the dissolution of olivine at 25 °C, which indicate that the enhanced H^+ ions available for leaching can increase the Mg content in leached solution and the silica content in the leached residue [37]. The pH of acid solutions used in this study range from 0.3 to 1.6. It is difficult to observe the differences at extremely low pH in a small range. The independence of acid concentration was also observed in the case of Mg leaching

from serpentine where acid concentration ranged from 0.5 to 4 M [38]. The unaltered Mg:Si ratios are the main reason for the constant interaction potential between CO_2 and the acid-treated olivine.

Although the CO_2 adsorption capacity per surface area of acid-treated olivine is lower than pristine olivine, the enlarged specific surface area made the CO_2 adsorption capacity of acid-treated olivine equal or greater than that of pristine olivine.

4.2. VSA of CO_2 on Pristine Olivine

Isotherm studies have indicated that VSA of CO_2 on pristine olivine is irreversible. Even though pristine olivine has a high CO_2 adsorption capacity, its expected working capacity for VSA is low because it is hard to regenerate. A similar shape of isotherms has been reported for metal organic frameworks (MOFs). An additional uptake of CO_2 on MOF in the presence of Mg-O bond has been shown at 0.1 bar and ambient temperature [14,31]. A full atomistic level study [39] has revealed that the adsorption mechanism for CO_2 on Mg-rich minerals consists of strong chemisorptions followed by physisorption. The chemical bond between Mg and CO_3 is much more difficult to break than van der Waals force. The isotherm model fits with our experimental data, indicating that chemisorption takes part in the CO_2 adsorption on pristine olivine, though physisorption dominates the process. The performance of olivine in the VSA process is mainly because of the existence of Mg complex on the surface of olivine.

From a thermodynamics point of view, 10^{-4} bar is the equilibrium CO_2 pressure in a Mg_2SiO_4-$MgCO_3$-CO_2 system at 25 °C [5]. Above the equilibrium pressure, CO_2 adsorption proceeds spontaneously, and below it the chemical reaction is reversed. In our studies, the outgas process breaks some chemical bond between CO_2 and MgO at 10^{-5} bar and 25 °C. However, breaking chemical bonds is time consuming, which conflicts with the benefit of VSA in quick CO_2 regeneration. Materials similar to pristine olivine are not ideal adsorbents for CO_2 separation by VSA.

Pristine olivine is a promising adsorbent for CO_2 capture at a low relative pressure, according to the isotherm EWC analysis. Representative flue gases are usually a mixture of N_2, CO_2, moisture, and other components, e.g., NO_x, with the CO_2 partial pressure of 0.05–0.2 bar, at around 25–75 °C [14]. The CO_2 concentration present in air is 400 ppm (CO_2 partial pressure of 4×10^{-4} bar) [40]. Integrate CO_2 capture and sequestration from flue gas and air will simplify the process and decrease the cost [6]. However, the other gas components in gas mixtures may compete or affiliate with CO_2 adsorption on the samples. Further studies on the adsorption of gas mixtures on olivine are needed to adapt to the actual situation.

4.3. VSA of CO_2 on Acid-Treated Olivine

Acid treatment on olivine changed the chemical and physical properties of the solid surface, and altered the CO_2 adsorption mechanism and application potential in the VSA process. During the process of acid leaching, Mg^{2+} was washed out and a porous silica passive layer was left on the surface of the olivine. Similar results have been observed in Bearat *et al.* [36]. CO_2 adsorption on acid-treated olivine presents a linear and reversible isotherm, which indicates that only physisorption happens during the process. CO_2 adsorption capacity for acid-treated olivine is stable during multi-cycle adsorption. Even though the acid-treated olivine with little Mg complex on the surface leads to a

decrease in CO_2 adsorption capacity per unit surface area, the increase in specific surface area enhances the CO_2 adsorption capacity per unit gram. The comparison of adsorption isotherm EMC indicates that acid-treated olivine is preferred as the CO_2 feed and regeneration pressure increases due to the linear shape of the isotherm. This result is in agreement with the study of Harlick and Tezel [34], which comprised various adsorbents for PSA application. The actual EWC of acid-treated olivine is much higher than pristine olivine. The reversible and stable isotherms indicate a potential for 100% recovery of CO_2 during the VSA process. All evidence shows that acid-treated magnesium silicate is more favorable than pristine magnesium silicate in VSA processes aimed at separation. Other features, such as CO_2 selectivity, tolerance to moisture and impurities, require further investigation.

4.4. Comparison with Literature Data

As analyzed above, the adsorption of CO_2 on OL and OL-A at 298 K are physisorption-dominated processes. For comparison, several physisorbents tested for VSA of CO_2 at room temperature are listed in Table 4. The lowest and the highest CO_2 partial pressure were chosen arbitrarily as 0.1 and 0.4 bar, respectively. The CO_2 adsorption capacities of OL and OL-A5 are considerably less than commonly used adsorbents, due to their small specific surface areas. However, the EWC per unit surface area of OL-A5 is higher than active carbon, and comparable to Mg/DOBDC and ZIF-78. Although, the value is less than Cu-BTC, Ni/DOBDC and Co/DOBDC, OL-A is competitive due to the simple sample preparation, as the acid-treated olivine could be the by-product of CO_2 mineralization sequestration. The EWC of OL is higher than OL-A5 at the evaluated VSA condition.

Table 4. CO_2 adsorption capacity on selected physisorbents material.

Sample Name	Type of Adsorbent	Surface Area (m²/g)	Temperature (°C)	A_{CO_2}[a] (mg/g)	EWC (mg/m²)	References
OL	Mineral	0.55	298	0.041–0.088[e]	0.078	This work
				0.065–0.103[f]	0.069	This work
OL-A5	Mineral	1.16	298	0.025–0.074	0.042	This work
NaX/1	Zeolite	-[d]	298	123.9–171.2	-[d]	[41]
Active carbon	Carbon	1300	298	26.3–65.8	0.030	[42]
Cu-BTC	MOF[b]	692	298	21.9–87.8	0.095	[43]
Ni/DOBDC	MOF	1080	296	118.5–175.6	0.053	[31]
Co/DOBDC	MOF	1070	296	122.9–235.3	0.105	[31]
Mg/DOBDC	MOF	1495	296	235.3–298.5	0.042	[31]
ZIF-78	ZIF[c]	620	298	33.8–60.0	0.042	[44]

a, CO_2 adsorption capacity at 0.1–0.4 bar (mg CO_2/g adsorbent); b, MOF is metal-organic framework; c, ZIF means Zeolitic Imidazolate Framework; d, Not given in literature; e, Data from adsorption isotherm; f, Data from desorption isotherm.

The optimum adsorbents for CO_2 separation from flue gas usually have a CO_2 adsorption capacity of 90–180 mg/g [13]. Even though the CO_2 adsorption capacities of OL and OL-A do not meet this requirement, they can be enhanced with the proper pretreatment method, by increasing the specific surface area of the samples. One potential pretreatment method is mechanical activation [45,46]. In

Fabian's study, 120-minute mechanically activated olivine with a specific surface area of 35.2 m^2/g, can adsorb a 3.2 mg CO_2/g sample at CO_2 partial pressure from a vacuum to 0.26 bar [45]. Another viable pretreatment method is chemical activation, by carefully choosing the agents. Chemical activation of serpentine using 5 M sulfuric acid creates a mesopore product with the specific surface area of 330 m^2/g [22]. If the same amount of surface area is obtained in acid-treated olivine, the CO_2 adsorption capacity can reach to 45.3 ± 0.7 mg/g at a CO_2 partial pressure of 1 bar. Except for pretreatment methods, the CO_2 adsorption capacity of olivine can be enhanced by increasing the temperature of adsorption, adding water content during the adsorption process [5]. In Kown's study, a maximum 180 mg of CO_2/g of olivine was obtained at 150 °C with 8.3 vol% H_2O in gas mixture [5]. However, the mechanism of CO_2 adsorption may change under high temperature and with the presence of moisture. Other silicates, such as serpentine, basalts and their constituent minerals, may also have the potential to be used in integrated CO_2 capture and sequestration. Since they have different crystal structure from olivine, an isotherm study on these materials is necessary to predict their application potential.

5. Conclusions

This paper analyzed the CO_2 sorption isotherm mechanism of pristine and acid-treated olivine, and estimates their application potential in a vacuum swing adsorption process for CO_2 capture. The Freundlich isotherm model produces the best fit for the CO_2 adsorption isotherm and the Temkin isotherm the best fit for the CO_2 desorption isotherm on pristine olivine. The CO_2 adsorption on both pristine and acid-treated olivine is mainly physisorption at 298 K. The change in CO_2 adsorption capacity is limited by the specific surface area, pore volume and the presence of Mg^{2+}. The actual EMC of adsorbents is a good indicator for industrial application, because it estimate both adsorption and desorption isotherms by considering CO_2 adsorption capacity and regenerability of the adsorbents.

Pristine olivine is not suitable for VSA of CO_2 due to its low actual EMC. However, it can be used in integrated CO_2 capture and sequestration, as it has a high CO_2 adsorption capacity even in diluted CO_2 concentration in feed gas. Alternately, acid-treated olivine is a promising adsorbent for CO_2 separation using the VSA process at relatively high CO_2 feed and regeneration pressure. The large specific surface areas (>330 m^2/g) produced by chemical treatment greatly enhances the CO_2 adsorption capacity of olivine and makes it a reasonable candidate for CO_2 capture by VSA process. The results of this study will provide primary consideration for process design in VSA processes of CO_2 on magnesium silicates.

Author Contributions

Both authors were involved in experimental design, laboratory work, manuscript writing and revising.

Conflicts of Interest

The authors declare no conflict of interest.

References

1. Intergovernmental Panel on Climate Change (IPCC). *Climate Change 2013: The Physical Science Basis*; Stocker, T.F., Qin, D., Plattner, G.-K., Tignor, M., Allen, S.K., Boschung, J., Nauels, A., Xia, Y., Bex, V., Midgley, P.M., Eds.; Cambridge University Press: Cambridge, UK and New York, NY, USA, 2013.

2. Yang, H.; Xu, Z.; Fan, M.; Gupta, R.; Slimane, R.B.; Bland, A.E.; Wright, I. Progress in carbon dioxide separation and capture: A review. *J. Environ. Sci.* **2008**, *20*, 14–27.

3. Werner, M.; Hariharan, S.; Zingaretti, D.; Baciocchi, R.; Mazzotti, M. Dissolution of dehydroxylated lizardite at flue gas conditions: I. Experimental study. *Chem. Eng. J.* **2014**, *241*, 301–313.

4. Hariharan, S.; Werner, M.; Hänchen, M.; Mazzotti, M. Dissolution of dehydroxylated lizardite at flue gas conditions: II. Kinetic modeling. *Chem. Eng. J.* **2014**, *241*, 314–326.

5. Kwon, S.; Fan, M.; DaCosta, H.F.M.; Russell, A.G. Factors affecting the direct mineralization of CO_2 with olivine. *J. Environ. Sci.* **2011**, *23*, 1233–1239.

6. Veetil, S.P.; Mercier, G.; Blais, J.F.; Cecchi, E.; Kentish, S. CO_2 sequestration by direct dry gas-solid contact of serpentinite mining residues: A Solution for industrial CO_2 emission. *Int. J. Environ. Pollut. Remediat.* **2014**, *2*, 52–59.

7. Kohlmann, J.; Zevenhoven, R. The removal of CO_2 from Flue gases using magnesium silicates, in Finland. In Proceedings of the 11th International Conference on Coal Science, San Francisco, CA, USA, 29 September–5 October 2001.

8. Power, I.M.; Harrison, A.L.; Dipple, G.M.; Wilson, S.A.; Kelemen, P.B.; Hitch, M.; Southam, G. Carbon mineralization: From natural analogues to engineered systems. *Rev. Mineral. Geochem.* **2013**, *77*, 305–360.

9. Zevenhoven, R.; Kohlmann, J. Direct Dry Mineral Carbonation for CO_2 Emissions Reduction in Finland. In Proceedings of the 27th International Technical Conference on Coal Utilization & Fuel Systems, Clearwater, FL, USA, 4–7 March 2002.

10. Kwon, S.; Fan, M.; Dacosta, H.F.M.; Russell, A.G.; Berchtold, K.A.; Dubey, M.K. CO_2 Sorption. In *Coal Gasification and Its Applications*; Elsevier: Amsterdam, The Netherlands, 2011; pp. 293–339.

11. Lowell, S.; Shields, J.E.; Thomas, M.A.; Thommes, M. *Characterization of Porous Solids and Powders: Surface Area, Pore Size, and Densit*; Kluwer Academic Publishers: Dordrecht, The Netherlands, 2004; p. 347.

12. Guthrie, G.D.; Carey, J.W.; Bergfeld, D.; Byler, D.; Chipera, S.; Ziock, H.; Lackner, K.S. *Geochemical Aspects of the Carbonation of Magnesium Silicates in an Aqueious Medium*; Los Alamos National Laboratory: Los Alamos, NM, USA, 1999; p. 14.

13. Ho, M.T.; Allinson, G.W.; Wiley, D.E. Reducing the cost of CO_2 capture from flue gases using pressure swing adsorption. *Ind. Eng. Chem. Res.* **2008**, *47*, 4883–4890.

14. Sayari, A.; Belmabkhout, Y.; Serna-Guerrero, R. Flue gas treatment via CO_2 adsorption. *Chem. Eng. J.* **2011**, *171*, 760–774.

15. Hedin, N.; Andersson, L.; Bergström, L.; Yan, J. Adsorbents for the post-combustion capture of CO_2 using rapid temperature swing or vacuum swing adsorption. *Appl. Energy* **2013**, *104*, 418–433.

16. Maring, B.J.; Webley, P.A. A new simplified pressure/vacuum swing adsorption model for rapid adsorbent screening for CO_2 capture applications. *Int. J. Greenh. Gas Control* **2013**, *15*, 16–31.

17. Seifritz, W. CO_2 disposal by means of silicates. *Nature* **1990**, *345*, 486.

18. Lackner, K.S.; Butt, D.P.; Wendt, C.H.; Ziock, H. *Mineral Carbonates as Carbon Dioxide Sinks*; Los Alamos National Laboratory: Los Alamos, NM, USA, 1999; p. 10.

19. Hitch, M.; Ballantyne, S.M.; Hindle, S.R. Revaluing mine waste rock for carbon capture and storage. *Int. J. Min. Reclam. Environ.* **2010**, *24*, 64–79.

20. Kwon, S. *Mineralization for CO_2 Sequstration Using Olivine Sorbent in the Presence of Water Vapor*; Georgia Institute of Technology: Atlanta, GA, USA, 2011; p. 181.

21. Alexander, G.; Maroto-Valer, M.M.; Gafarova-Aksoy, P. Evaluation of reaction variables in the dissolution of serpentine for mineral carbonation. *Fuel* **2007**, *86*, 273–281.

22. Maroto-valer, M.M.; Fauth, D.J.; Kuchta, M.E.; Zhang, Y.; Andre, J.M. Activation of magnesium rich minerals as carbonation feedstock materials for CO_2 sequestration. *Fuel Process. Technol.* **2005**, *86*, 1627–1645.

23. Gadikota, G.; Natali, C.; Boschi, C.; Park, A.-H.A. Morphological changes during enhanced carbonation of asbestos containing material and its comparison to magnesium silicate minerals. *J. Hazard. Mater.* **2014**, *264*, 42–52.

24. Gadikota, G.; Swanson, E.J.; Zhao, H.; Park, A.-H.A. Experimental design and data analysis for accurate estimation of reaction kinetics and conversion for carbon mineralization. *Ind. Eng. Chem. Res.* **2014**, *53*, 6664–6676.

25. Gadikota, G.; Kelemen, P.; Matter, J.; Park, A.-H.A. Chemical and morphological changes during olivine carbonation for CO_2 Storage in the presence of NaCl and $NaHCO_3$. *Phys. Chem. Chem. Phys.* **2014**, *16*, 4679–4693.

26. Gadikota, G.; Park, A.-H.A. Accelerated carbonation of Ca- and Mg-bearing minerals and industrial wastes using CO_2. In *Carbon Dioxide Utilization: Closing the Carbon Cycle*; Elsevier: Amsterdam, The Netherlands, 2014.

27. Hänchen, M.; Prigiobbe, V.; Storti, G.; Seward, T.M.; Mazzotti, M. Dissolution kinetics of fosteritic olivine at 90–150 °C including effects of the presence of CO_2. *Geochim. Cosmochim. Acta* **2006**, *70*, 4403–4416.

28. Soares, J.L.; Casarin, G.L.; Jose, H.J.; Moreira, R.D.; Rodrigues, A.E. Experimental and Theoretical Analysis for the CO_2 Adsorption on Hydrotalcite. *Adsorption* **2005**, *11*, 237–241.

29. Raudsepp, M.; Pani, E. Application of Rietveld analysis to environmental mineralogy. In *Environmental Mineralogy of Mine Wastes, Mineralogical Association of Canada Short Course*; Jambor, J.L., Blowes, D.W., Ritchie, A.I.M., Eds.; Mineralogical Association of Canada: Ottawa, ON, Canada, 2003; pp. 165–180.

30. Presnali, D.C.; Walter, M.J. Melting of forsterite, Mg_2SiO_4, From 9.7 to 16.5 GPa. *J. Geophys. Res.* **1993**, *98*, 19777–19783.

31. Caskey, S.R.; Wong-Foy, A.G.; Matzger, A.J. Dramatic tuning of carbon dioxide uptake via metal substitution in a coordination polymer with cylindrical pores. *J. Am. Chem. Soc.* **2008**, *130*, 10870–10871.

32. Ozkaya, B. Adsorption and desorption of phenol on activated carbon and a comparison of isotherm models. *J. Hazard. Mater.* **2006**, *129*, 158–163.

33. Itodo, A.U.; Itodo, H.U. Sorption energies estimation using Dubinin-Radushkevich and Temkin adsorption isotherm. *Life Sci. J.* **2010**, *7*, 31–39.

34. Harlick, P.J.E.; Tezel, F.H. An experimental adsorbent screening study for CO_2 removal from N_2. *Microporous Mesoporous Mater.* **2004**, *76*, 71–79.

35. Haug, T. *Dissolution and Carbonation of Mechanically Activated Olivine*; Norwegian University of Science and Technology: Trondheim, Norway, 2010; p. 243.

36. Béarat, H.; McKelvy, M.J.; Chizmeshya, A.V.G.; Gormley, D.; Nunez, R.; Carpenter, R.W.; Squires, K.; Wolf, G.H. Carbon sequestration via aqueous olivine mineral carbonation: role of passivating layer formation. *Environ. Sci. Technol.* **2006**, *40*, 4802–4808.

37. Rimstidt, J.D.; Brantley, S.L.; Olsen, A.A. Systematic review of forsterite dissolution rate data. *Geochim. Cosmochim. Acta* **2012**, *99*, 159–178.

38. Zhang, Q.; Sugiyama, K.; Saito, F. Enhancement of acid extraction of magnesium and silicon from serpentine by mechanochemical treatment. *Hydrometallurgy* **1997**, *45*, 323–331.

39. Kwon, S.; Choi, J., II; Lee, S.G.; Jang, S.S. A density functional theory (DFT) study of CO_2 adsorption on Mg-rich minerals by enhanced charge distribution. *Comput. Mater. Sci.* **2014**, *95*, 181–186.

40. Keeling, R. Scripps Institution of Oceanography. Available online: http://scrippsco2.ucsd.edu/ (accessed on 20 December 2014).

41. Cavenati, S.; Grande, C.A.; Rodrigues, A.E. Adsorption equilibrium of methane, carbon dioxide, and nitrogen on zeolites 13X at high pressures. *J. Chem. Eng. Data* **2004**, *49*, 1095–1101.

42. Na, B.K.; Koo, I.K.; Eum, H.M.; Lee, H.; Song, H.K. CO_2 recovery from flue gas by PSA process using activated carbon, Korean. *J. Chem. Eng.* **2001**, *18*, 220–227.

43. Yang, Q.; Xue, C.; Zhong, C.; Chen, J.F. Molecular simulation of separation of CO_2 from flue gas in Cu-BTC metal-organic framework. *AIChE J.* **2007**, *53*, 2832–2840.

44. Phan, A.; Doonan, C.J.; Uribe-Romo, F.J.; Knobler, C.; O'Keeffe, M.; Yaghi, O.M. Synthesis, structure, and carbon dioxide of zeolitic imidazolate frameworks. *Acc. Chem. Res.* **2010**, *43*, 58–67.

45. Fabian, M.; Shopska, M.; Paneva, D.; Kadinov, G.; Kostova, N.; Turianicová, E.; Briančin, J.; Mitov, I.; Kleiv, R.A.; Baláž, P. The influence of attrition milling on carbon dioxide sequestration on magnesium–iron silicate. *Miner. Eng.* **2010**, *23*, 616–620.

46. Hangx, S.J.T.; Spiers, C.J. Coastal spreading of olivine to control atmospheric CO_2 concentrations: A critical analysis of viability. *Int. J. Greenh. Gas Control* **2009**, *3*, 757–767.